DOI: 10.1002/ejoc.200900338

Efficient Regiospecific Conjugated Ring Fusion in N-Confused Porphyrin

Piotr J. Chmielewski,*[a] Justyna Maciołek,[a] and Ludmiła Szterenberg[a]

Keywords: Porphyrinoids / Aromaticity / Macrocycles / Fused ring systems

Acid-catalyzed exocyclic ring formation in *meso*-tetrakis(3′,5′-dimethoxyphenyl)-2-aza-21-carbaporphyrin takes place regioselectively between the external carbon atom of the confused pyrrole and the *ortho*-carbon atom of the adjacent *meso*-aryl group. The ring fusion strongly alters the spectroscopic properties of the macrocycle, but its aromaticity is preserved, as shown by NMR spectroscopy as well as DFT calculations. A tendency to self-associate is observed for partially protonated and nickel(II)-metalated systems. A novel silver(I)-bridged dimer is formed in the reaction of the fused carbaporphyrin with $AgBF_4$. Cyclic voltammetry studies of this system indicate an interaction between the subunits.

Introduction

Modification of porphyrin by fusion of an additional ring onto the macrocycle's perimeter can lead to a profound alteration of its optical, coordination, or redox properties. It is particularly efficient when the π-bonding systems of the macrocyclic and external rings are conjugated. Several synthetic routes from porphyrin to its derivatives bearing a fused ring have been developed.[1] The exocyclic ring can be fused to pyrrole alone or link the β-pyrrole and the *meso*-aryl substituents.[2] The fusion of several porphyrin subunits has also been exploited for the efficient synthesis of porphyrin arrays.[3] In the case of the porphyrin isomer, N-confused porphyrin (NCP),[4,5] derivatives containing additional rings have been obtained by taking advantage of the peculiar reactivity of the confused pyrrole.[6–9] Inversion of the confused pyrrole leads to the formation of an N-fused porphyrin, which has been recently reported as an intermediate in the synthesis of several derivatives of NCP.[10] Some of the fused systems remain aromatic, whereas in others either the macrocyclic conjugation path is interrupted[9] or the oxidation state prevents the occurrence of a diatropic current.[11] In all the NCP derivatives containing a fused ring that have been reported to date, either the internal or external nitrogen atom is involved in the fusion. In this paper we report the synthesis and characterization of the first example of an NCP bearing a fused ring formed on the macrocyclic perimeter that involves only carbon atoms. This type of modification should retain both internal and external donor sites of the macrocycle, and thus the basic and coordination properties of the fused system are also of interest as well as the alteration of the spectroscopic properties of the macrocycle introduced by the external ring fusion.

Results and Discussion

Protonation of the external and internal nitrogen atoms of NCP has been shown to result in a distinct reactivity of the "external" carbon atom C-3 of the confused pyrrole leading to C–C bond formation with C-3 of another NCP molecule[12] or with an α-carbon atom of free pyrrole.[13] The activation of this reaction site by an acid can be interpreted as increasing the electrophilic character of C-3. Clearly, the C–C bond formation requires the presence of an accessible nucleophilic carbon atom. The presence of an oxidant (air or quinone derivative) is necessary to quench the equilibrium of the reversible C–C bond formation by the dehydrogenation of both bond-forming carbon atoms.

We decided to apply this approach in our efforts to modify NCP by fusion of the adjacent *meso*-aryl ring. To increase the nucleophilic character of the *ortho*-carbon atoms of the aryl substituent in the 5-position of the porphyrin ring, electron-donating substituents were introduced. In all but one system, the only product of the reaction after 48 h of reflux was the dimeric NCP **3** (Scheme 1),[12] which was formed in a yield of 5–70%, depending on the substituent. Only the reaction of 5,10,15,20-tetrakis(3′,5′-dimethoxyphenyl)-2-aza-21-carbaporphyrin {**1**-[3′,5′-$(OMe)_2$]} in a toluene solution acidified with trifluoroacetic acid (TFA) in the presence of atmospheric oxygen under reflux resulted after about 5 h in the formation of a red product in a yield of 70% identified as *C*-fused NCP **2** (Scheme 1). After chromatographic workup, the compound was characterized by standard methods, including homo- and heteronuclear 1D and 2D NMR techniques, allowing full assignment of all

[a] Department of Chemistry, University of Wrocław,
14 F. Joliot-Curie Street, 50383 Wrocław, Poland
E-mail: pjc@wchuwr.pl
Supporting information for this article is available on the WWW under http://dx.doi.org/10.1002/ejoc.200900338.

NMR signals. The molecular mass of **2** (m/z = 853) is two units smaller than that of the parent porphyrin **1**-[3′,5′-$(OMe)_2$], which indicates the loss of two hydrogen atoms, in line with the structure of the product. No dimeric porphyrin formation was observed for this system.

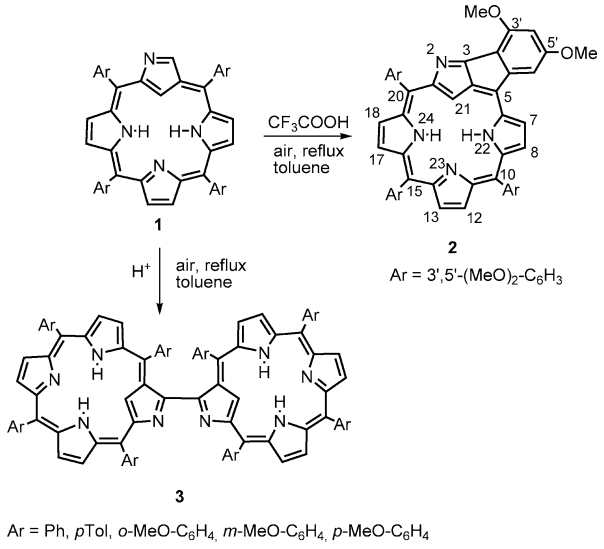

Scheme 1. Alternative reaction paths of NCP under acidic conditions.

The conversion of NCP **1**-[3′,5′-$(OMe)_2$] into its *C*-fused derivative **2** was carried out under the conditions of acid-catalyzed condensation, which otherwise results in the dimer $(NCP)_2$ (**3**; Scheme 1).[12] To rationalize the factors determining the reaction path, we estimated the charge distribution among the atoms in the free base and dicationic forms of the DFT-optimized structures of tetrakis(*p*-tolyl)- and tetrakis(3′,5′-dimethoxyphenyl)-NCP.[14] The natural population analysis (NPA) approach applied to these models indicates that protonation of the external and internal nitrogen atoms decreases the electron density on the 3-CH fragment in both macrocycles, which is reflected by the increase in the partial charge on this site from +0.205 in the free bases to +0.341 in the dicationic forms. The predicted decrease in the electron density makes this site more susceptible to the reaction with nucleophiles. The partial charge on the *o*-CH group of the aryl substituents in the 5-position is not considerably altered by the protonation, but it depends on the ring substitution. For **1**-(*p*-Tol) the average sum of the charges on the carbon atoms and protons in both the *ortho* positions is –0.009 in the neutral form and –0.001 in the dicationic form, whereas for **1**-[3′,5′-$(OMe)_2$] the charges are –0.060 and –0.063, respectively. The significantly higher electron density on these sites seems to be responsible for the different reactivity of **1**-[3′,5′-$(OMe)_2$]. It appears that the *ortho*-carbon atoms of the aryl group in the *meso* 5-position [i.e., carbon atoms C-5(2′) and C-5(6′)] are sufficiently activated towards interaction with the electrophilic carbon atom at the 3-position only in the case of the system with two electron-donating methoxy substituents in the *ortho* and *para* positions with respect to the potential reaction sites.

The ^{1}H NMR spectrum of the macrocyclic ring of **2** ($CDCl_3$, 213 K, Figure 1A) consists of six signals of β-pyrrole protons in the region of δ = 7.6–8.2 ppm, two NH signals (δ = 1.93 and 2.26 ppm) assigned on the basis of isotopic substitution by D_2O and correlation with appropriate pyrrole protons in a COSY experiment, and the 21-H signal at δ = –0.66 ppm. Importantly, no signal from the proton at the 3-position, that is, that attached to the external car-

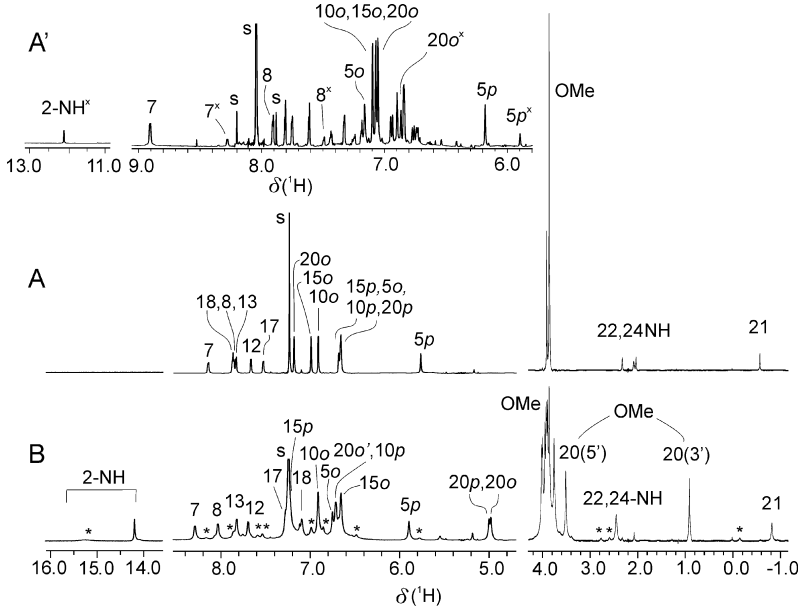

Figure 1. ^{1}H NMR spectra (500 MHz, $CDCl_3$, 213 K) of **2** (trace A) and $[(\mathbf{2})_2H]^+$ (trace B, recorded upon addition of 0.7 equiv. of TFA; the weak signals of the coexisting monocation $[\mathbf{2}H]^+$ are marked with asterisks). The signal assignments follow the numbering given in Scheme 1. The inset A′ contains low-field fragments of the spectrum of **2** recorded in $[D]_7$DMF at 213 K. The selected signals of the minor tautomer **2a** are marked with the symbol ^{x}.

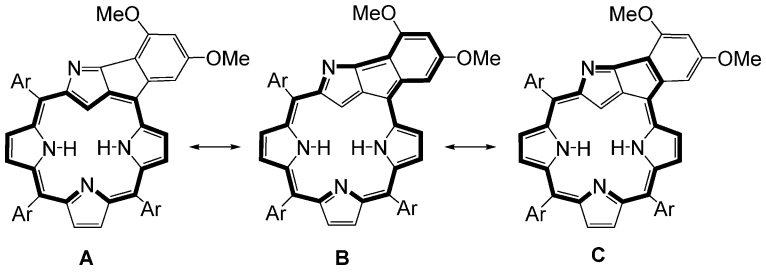

Scheme 2. Resonance structures of **2**.

bon atom of the confused pyrrole of NCP, can be observed in the spectrum of **2**. The doublets at δ = 6.96, 7.03, and 7.21 ppm are due to three pairs of equivalent *ortho* protons of the 3′,5′-dimethoxyphenyl substituents in the *meso* 10-, 15-, and 20-positions, and the three triplets at δ = 6.71, 6.69, and 6.67 ppm are the signals of the corresponding *para* protons. The *ortho* and *para* protons of the aryl group in the 5-position, that is, the ring fused to the macrocycle, appear as doublets at δ = 6.73 and 5.82 ppm. The upfield shift of these signals reflects changes in the electron density distribution among the carbon atoms in the six-membered ring and a reduction of the aromatic ring current caused by fusion. Also, the aromaticity of the macrocyclic ring is affected by the formation of the additional ring, as can be inferred on the basis of the upfield shift of the β-pyrrole protons (by about 1 ppm) and the downfield shift of the internal NH an CH protons (by more than 4 ppm) with respect to the parent NCP.

The effective inclusion of six or two additional π electrons into the delocalization path in **2**, schematically represented by the canonic forms **B** and **C** in Scheme 2, should result in 24 or 20 π-electron conjugated systems and a paratropic ring current, yet the compound remains aromatic, as can be inferred from the NMR spectra. This is in accord with the aromaticity index NICS (–8.17) as well as the proton and carbon chemical shifts (Figure 2) calculated for the DFT-optimized structure of **2** (Figure 3) at the B3LYP/6-31G** level of theory,[14] which indicates the presence of diatropic current in the macrocyclic ring.

The optical spectrum of **2** (Figure 4) is markedly different to those of **1** and its 2-substituted derivatives.[4,15] The split Soret band may reflect the contribution of the fused rings to the aromatic system of the macrocycle. Similar splitting has been observed previously for *N*-fused porphyrin[6] and isoquinolinocarbaporphyrin.[8] Less pronounced effects of this type have been reported for 3-(2′-pyrrole)-substituted NCP[13] or for the dimer **3**.[12a]

Fusion introduces several alterations with respect to the starting NCP. One is the less effective tautomerization in polar solvents to the form **2a** (Scheme 3).[16] Thus, unlike in the case of **1**, the electronic spectra of **2** in dichloromethane or DMF are very similar, which suggests a lack of proton transfer from the porphyrin core to its perimeter. On the other hand, a close inspection of the ^{1}H NMR spectrum of **2** in [D$_7$]DMF reveals the presence of a certain amount (about 20%) of a less aromatic tautomer with a signal at δ = 12.1 ppm (213 K) due to the presence of a proton on the external nitrogen atom N-2 (Figure 1A′). The weak signals from other protons of **2a** can be identified by chemical exchange correlations with the corresponding protons of the main component observed in the ROESY map at room temperature (see the Supporting Information).

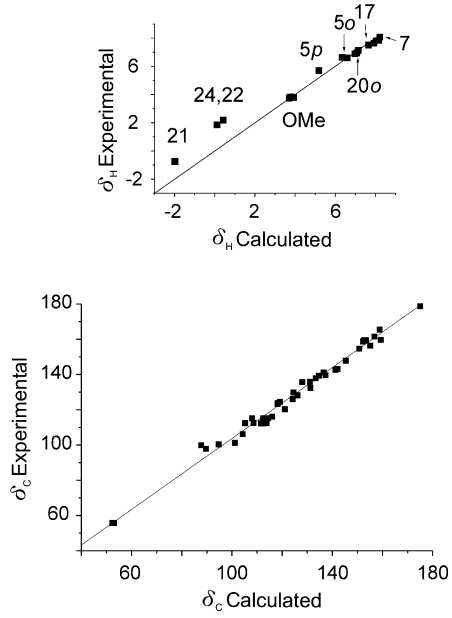

Figure 2. Correlation diagrams of calculated and experimental ($CDCl_3$, 298 K) values of ^{1}H (top) and ^{13}C (bottom) chemical shifts of **2**.

Also, protonation of **2** (Scheme 4) proceeds with a different pattern to that of **1**.[4] The ^{1}H NMR titration of **2** with TFA at a low temperature ($CDCl_3$, 213 K) reveals the formation of a dimer $[(\mathbf{2})_2H]^+$ with the subunits linked by a hydrogen bond between external nitrogen atoms that is symmetric on the NMR timescale (Figure 1B). The dimer dominates in solutions containing 0.3–1 equiv. of the acid, but is also present at higher TFA concentrations coexisting with the mono- and dicationic forms $[\mathbf{2}H]^+$ and $[\mathbf{2}H_2]^{2+}$. The ^{1}H NMR spectrum of $[(\mathbf{2})_2H]^+$ exhibits features typical of β-β linked bis(tetraarylporphyrins).[12,17] That includes a strong high-field shift of signals of protons located in the vicinity of the bridge, that is, one of the *ortho* protons of the aryl group at the *meso* 20-position, the corresponding *para* proton, and one methoxy group of the substituent in

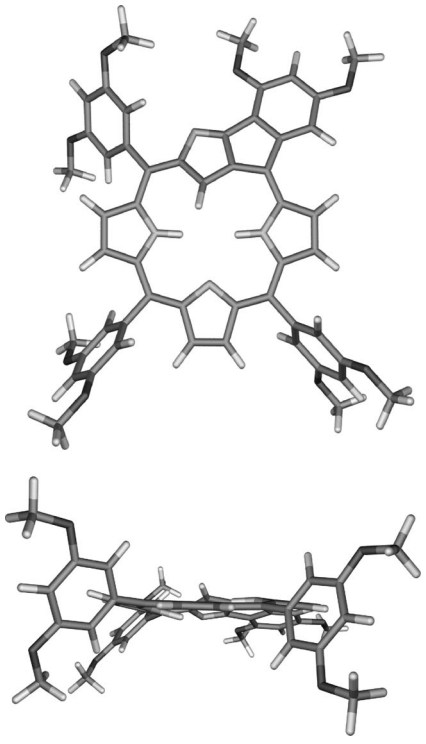

Figure 3. Two projections of the DFT-optimized structure of **2**.

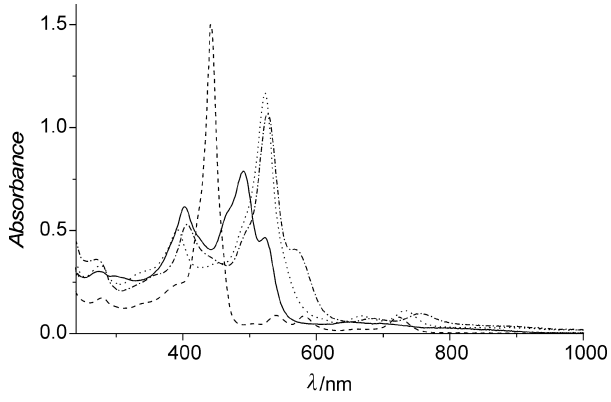

Figure 4. Optical spectra of dichloromethane solutions of **1** (dashed line), **2** (solid line), its monocation (dotted line), and the dication (dash-dot line).

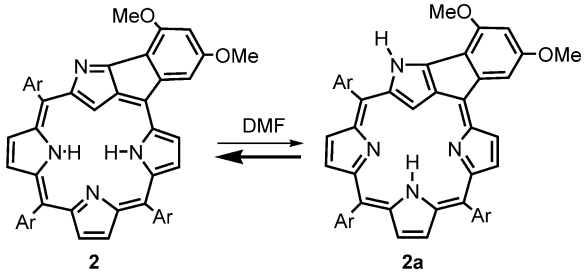

Scheme 3. Tautomeric equilibrium of **2** in DMF.

the 20-position. These effects are caused by a shielding effect of the aromatic ring current of the neighboring subunit. Unlike in the free base or higher protonated forms, for which five methoxy resonances are observed owing to the effectively planar structure of the macrocycle, in the case of $[(\mathbf{2})_2H]^+$ there are eight signals from the methoxy groups. Differentiation of the chemical shifts of all the methoxy substituents reflects a nonplanar structure of the adduct. A strongly downfield-shifted position of the 2-NH signal (δ = 14.2 ppm) indicates involvement of this proton in a hydrogen bond, whereas the relative integral peak intensity (1:2 with respect to 21-H or 7-H) reveals the unique character of the bridging proton.

The through-space interaction between the "internal" protons (21-H, 22-H, 24-H) and the methoxy or aryl protons of the substituent at the 20-position observed in the NOESY and ROESY spectra of $[(\mathbf{2})_2H]^+$ are in line with a dimeric structure. The DFT (B3LYP/6-31G**)-optimized structure (Figure 5) presents an arrangement of the subunits in $[(\mathbf{2})_2H]^+$ in which this kind of interprotonic interaction can be effective.[14] Also the proton chemical shifts calculated for this model reflect the shielding effect of aromatic current on the resonances of the substituent at the 20-position as well as the involvement of 2-NH in the hydrogen bond between the subunits (see the Supporting Information for details). Significantly, a positive-ion ESI TOF mass spectrum of the acidified solution of **2** includes a peak at m/z = 1706, which indicates the presence of a dimer. No such dimerization can be observed upon protonation of the parent porphyrin **1**-[3′,5′-$(OMe)_2$], from which the importance of fusion in the association can be inferred.

The spectrophotometric titration of **2** with TFA at room temperature reveals, however, the formation of only two protonated species in solution (Figure 4), which may be a result of the similarity of the spectral responses of the monocation and its hydrogen-bonded associate with the free base.

Insertion of the nickel(II) ion into the macrocycle **2** requires harsher conditions than is the case with unaltered NCP or its *N*-substituted derivatives.[4,15,18] The nickel complex **4** was obtained after heating a toluene/ethanol solution of **2** with an excess of nickel(II) acetate under nitrogen at reflux for 12 h (Scheme 3). The purple-red air-stable diamagnetic and neutral complex was separated on a column of silica gel and characterized by mass spectrometry, UV/Vis spectrophotometry, and NMR spectroscopy. The ^1H NMR spectrum of **4** (Figure 6, $CDCl_3$, 298 K) indicates deprotonation of the internal nitrogen atoms and C-21 and the presence of a proton on the external nitrogen atom N-2, as in the case of the nickel(II) complex of NCP.[4] However, in the case of **4** only residual macrocyclic aromaticity can be observed with the signals of the β-pyrrole protons in the region of δ = 6.95–7.35 ppm. Also, the signal of 2-H at δ = 7.6 ppm is shifted by about 2.5 ppm upfield with respect to its position observed for NCP nickel(II) complexes.

The ESI TOF mass spectrum of **4** indicates the presence of a molecular ion of m/z = 908.3, in line with the composition of the compound; however, it also exhibits other signals representing various associate molecules. These include strong peaks of the monocationic dimer at m/z = 1818.5, a

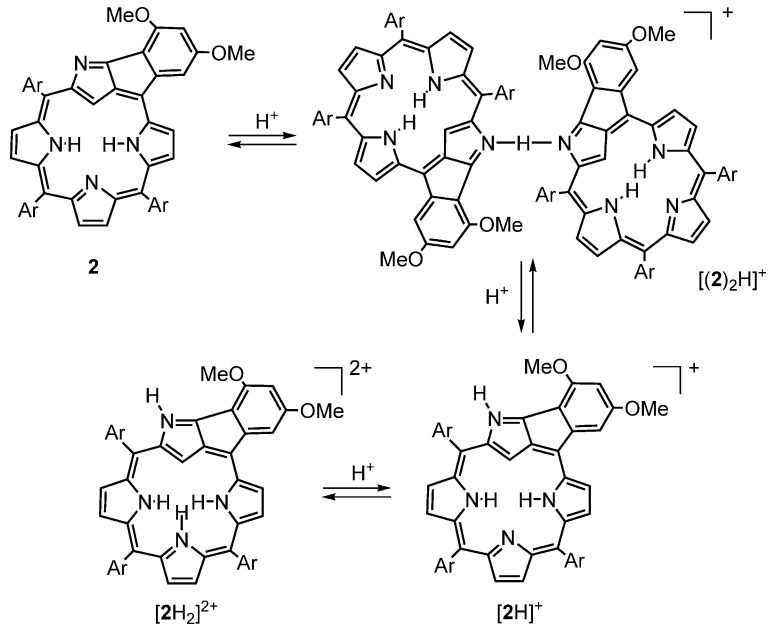

Scheme 4. Stepwise protonation of **2**.

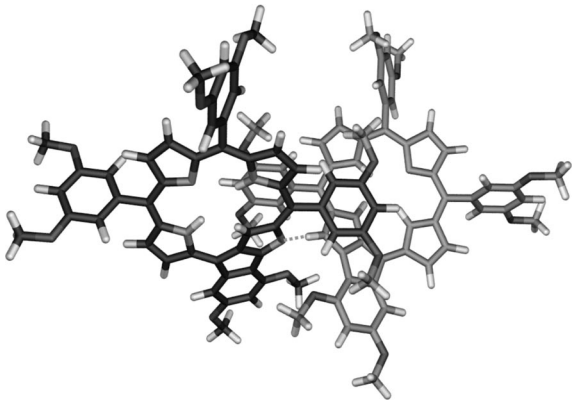

Figure 5. DFT-optimized structure of $[(\mathbf{2})_2H]^+$ presenting an overlap of the subunits and hydrogen-bond formation (dotted line).

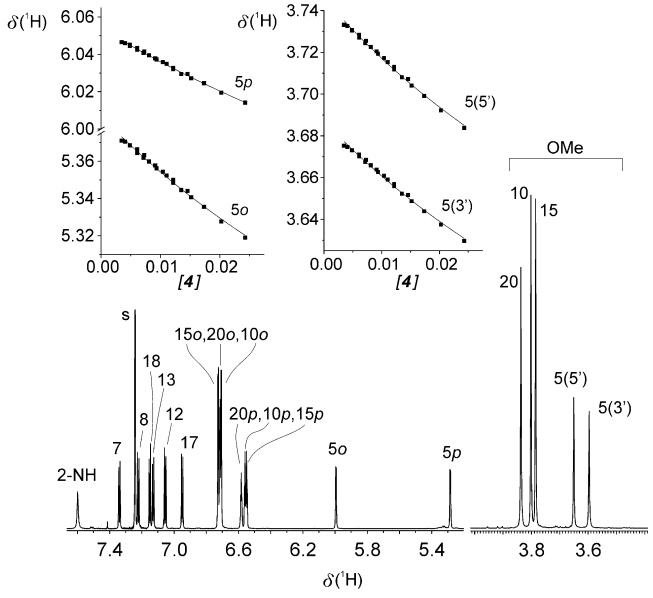

Figure 6. ^{1}H NMR spectrum and signal assignments for **4** (600 MHz, $CDCl_3$, 298 K). The insets show the concentration dependence of the chemical shift of the four proton groups. The solid curves were calculated on the basis of a least-squares analysis of the experimental data, assuming the formation of a dimeric assembly.

trimer at *m*/*z* = 2728, a dicationic pentamer at *m*/*z* = 2273, and traces of a tricationic octamer at *m*/*z* = 2425. We believe that association is responsible for the slow precipitation of **4** from solution in dichloromethane or chloroform, which takes place at room temperature at concentrations even as low as 0.02 M. For the $CDCl_3$ solutions there is a distinct concentration dependence of the NMR chemical shifts of the *ortho* and *para* 5-aryl protons and the 5(3′)- and 5(5′)-methoxy protons (Figure 6). The positions of the other peaks in the ^{1}H NMR spectrum of **4** either do not vary with concentration or the dependence of their chemical shifts is much weaker (protons 7-H and 8-H). The selectivity of the dependence as well as the upfield shift of the signals with increasing concentration suggest that the intermolecular contacts occur in the region of the fused rings. Assuming the formation of the dimer $(\mathbf{4})_2$ in the first stage of the association we estimate the equilibrium constant for the dimerization as 6(1) M^{-1} at 298 K on the basis of a non-linear least-squares analysis of the experimental data. In the total concentration range of **4** (0.002–0.024 M) the molar ratio of the associate varies from 0.01 to about 0.1.

In the case of porphyrin **1** and many of its derivatives, the reaction with silver(I) salts carried out under mild conditions yields stable organometallic diamagnetic silver(III) complexes with the metal ion inserted into a fully deprotonated macrocyclic cavity.[8,12b,12c,18,19] Our attempt at silver insertion into **2** by using silver(I) acetate or trifluoroacetate in various solvents resulted in several ill-defined nonaro-

matic products. On the other hand, mixing of a chloroform solution of **2** with solid $AgBF_4$ yields, after deacidification with water, an orange-red product that can be identified as complex **5** (Scheme 5) and consists of two subunits linked by the coordination of a silver(I) ion.

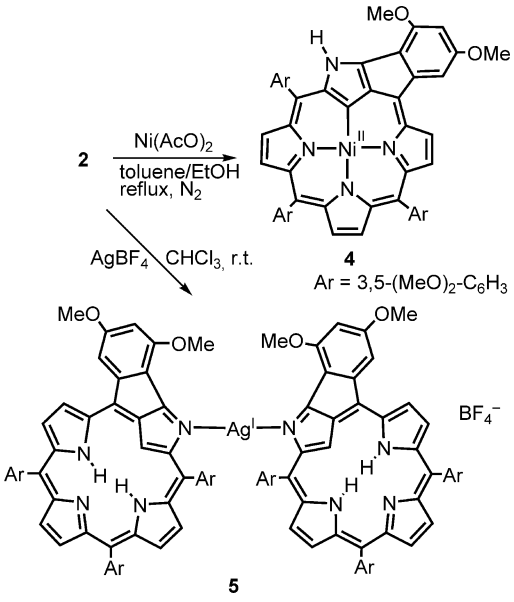

Scheme 5. Metalation of **2** with nickel(II) and silver(I).

The formulation of product **5** as a bis(porphyrin)silver(I) complex relied on mass spectrometry, multinuclear NMR, and UV/Vis data. The ESI TOF mass spectrum of **5** consists of a signal at m/z = 1813.5, which reflects the presence of a positively charged complex containing two unaltered units of **2** and one silver ion. This is in line with the ^{1}H NMR spectrum of **5**, which displays the full set of signals expected for **2** (Figure 1A), including the presence of signals of 22-H, 24-H, and 21-H, with some significant differences. First of all the symmetry plane that is present in **2** is lost in **5** because each of the aryl protons resonate at different frequencies. Also, each of the methoxy groups gives distinct signals (Figure 7) unlike in the case of **2** for which these signals are pairwise degenerated within each of the *meso* substituents owing to the planar structure of the macrocycle. This indicates that **5** is nonplanar. The effective molecular symmetry is C_2 on the basis of its dimeric structure. A selective upfield shift of the signals of one of the methoxy groups (by about 2.5 ppm), one of the *ortho* protons, and the *para* proton (by more than 1 ppm) of the substituent at the *meso* 20-position caused by the aromatic ring current of the neighboring subunit reveals the orientation of the macrocyclic rings. Also, the through-space interactions between the protons of the substituent at the 20-position and the "internal" protons at the 21-, 22-, and 24-positions observed in the NOESY and ROESY experiments are in line with a structure consisting of two aromatic subunits that are in contact through a bridge linking the external nitrogen atoms. In essence, the spectral pattern as well as the interprotonic contacts for **5** resemble that of the dimeric species $[(\mathbf{2})_2H]^+$ (Figure 1B) except for the obvious lack of a signal from the bridging proton. This suggests a linear arrangement of the N–Ag–N fragment, as in the case for the hydrogen-bonded nitrogen atoms in $[(\mathbf{2})_2H]^+$ (Figure 5). The more pronounced aromatic ring-current effects observed in the ^{1}H NMR spectrum of the system with the proton bridge compared with those of the bridging Ag^+ may be interpreted in terms of an ion-size difference that strongly influences the distance between the subunits.

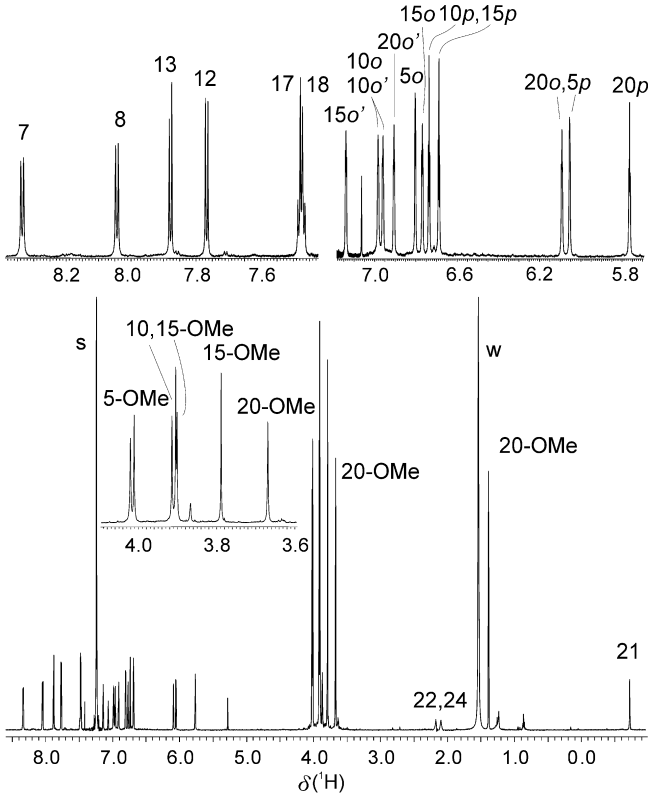

Figure 7. ^{1}H NMR spectrum and signal assignments for **5** (600 MHz, $CDCl_3$, 298 K). The insets show enlargements of various regions of the spectrum. The atom numbering follows that given in Scheme 1; s: solvent; w: dissolved water signal.

The dimeric structure of **5** is also reflected by a decrease in the diffusion coefficient D compared with that of the monomeric macrocycle **2**. Independent DOSY experiments performed on $CDCl_3$ solutions of both systems at 300 K (Figure 8) reveal about a 25% slower migration of the molecules in the case of the dimer, which is caused by its considerably higher molecular mass and size.[20] For the nickel(II) complex **4** the DOSY experiment gives the same diffusion coefficient as in the case of **2**, which is in line with a predominately monomeric character of this system.

The presence of the silver ion in the complex can be inferred from the ^{13}C NMR spectrum of **5** in which certain signals display splitting caused by the spin-spin coupling of the ^{107,109}Ag nuclei with adjacent carbon nuclei. Thus, the signal of C-21 at δ = 109.6 ppm, which can be unequivocally identified by ^{1}H,^{13}C HMQC experiments, is a doublet with a coupling constant of $^3J_{Ag,C}$ = 4.6 Hz. Two other signals (δ = 154.3 and 146.1 ppm), which correlate with 21-H in the ^{1}H,^{13}C HMBC experiments and on this basis can be

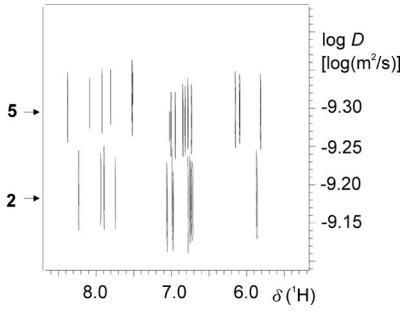

Figure 8. Superimposed fragments of the DOSY spectra (600 MHz, $CDCl_3$, 300 K) of **2** and **5**.

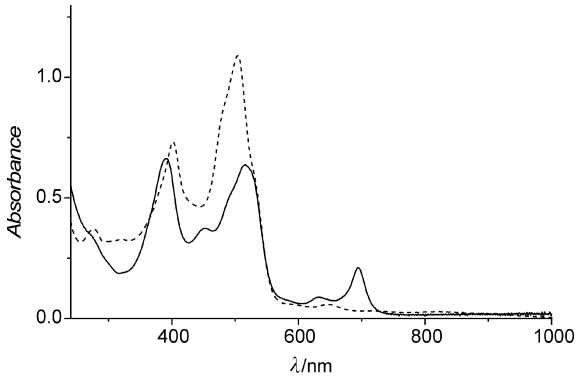

Figure 9. Optical spectra of dichloromethane solutions of **4** (solid line) and **5** (dashed line).

attributed to the confused pyrrole, are also split into doublets with a coupling constant of 6.4 Hz. Another doublet at δ = 142.4 ppm ($^3J_{Ag,C}$ = 4.7 Hz) can be assigned to the *meso* C-20 atom because it correlates with the neighboring pyrrole proton 7-H in the HMBC spectrum. The effects of multibonding ^{107,109}Ag,^{13}C coupling have been observed previously for silver(III) complexes and comprise the metal ion coordinated inside a macrocyclic cavity.[8] The complex is positively charged because it comprises a bridging cation as a structural fragment and thus requires a counteranion. Because silver(I) has been introduced as a trifluoroborate salt, the BF_4^- ion is expected to neutralize the charge of the assembly. Indeed, a singlet peak at δ = –163 ppm in the ^{19}F NMR spectrum of **5** (473 MHz, $CDCl_3$, 300 K) indicates the presence of the trifluoroborate counteranion.

The optical spectrum of **5** is considerably different to that of the nickel(II) complex **4** in dichloromethane, which reflects dissimilar patterns of metal ligation (Figure 9). In fact, the spectrum of **5** resembles that of the monoprotonated species that appears during the spectrophotometric titration with TFA (Figure 4). However, the spectrum of the silver-bridged assembly remains unaltered after washing the solution with water, unlike the case of the protonated species for which such treatment restores the free base **2**. On the other hand, the addition of dry tetraalkyl chloride to the dichloromethane solution of **5** resulted in a spectrum identical to that of uncomplexed macrocycle **2**, which indicates demetalation. This is additional proof for the presence of a silver(I) ion in **5**.

The redox properties of compounds **2**, **4**, and **5** were studied by cyclic voltammetry in dichloromethane solution, and the potentials were referenced to a ferrocene/ferrocenium internal standard. The voltammogram of the free base **2** consists of two oxidation (o1 at 159 mV and o2 at 468 mV) and two reduction couples (r1 at –1380 mV and r2 at –1910 mV) that are irreversible or quasi-reversible (Figure 10B). The values of the redox potentials fall in the range typical of porphyrin or other aromatic macrocycles, including N-confused analogues. However, a significant decrease (by about 340 mV) in the difference between the potentials of the first reduction and the first oxidation is observed for **2** compared with the parent compound **1**-[3′,5′-$(OMe)_2$] (Figure 10A). The cathodic shift of o1 and o2 and the anodic shift of r1 and r2 reflect the stabilization of the oxidized and reduced forms of the macrocycle caused by the extension of the delocalized π-orbital system in **2**. The first oxidation potential of the nickel(II) complex **4** is even more shifted towards a lower potential ($E^{o1}_{1/2}$ = 35 mV, Figure 10C) owing to the involvement of the metal d orbitals in the HOMO. Indeed, the EPR signal characteristic of a trivalent nickel complex is observed in the chemical oxidation of **4** with 1 equiv. of Br_2,[21] which indicates a metal-centered oxidation. The potentials of the second oxidation (520 mV) and the first reduction of **4** (–1312 mV) only slightly differ from those of **2**. However, an unexpected feature is observed for the second reduction of **4**. The wave is split into two weaker well-separated quasi-reversible couples at –1852 and –2000 mV. This may reflect an interaction between the subunits of the adduct that is formed on the electrode surface and consists of the anion radical formed upon the r1 process. The effects of an interaction between

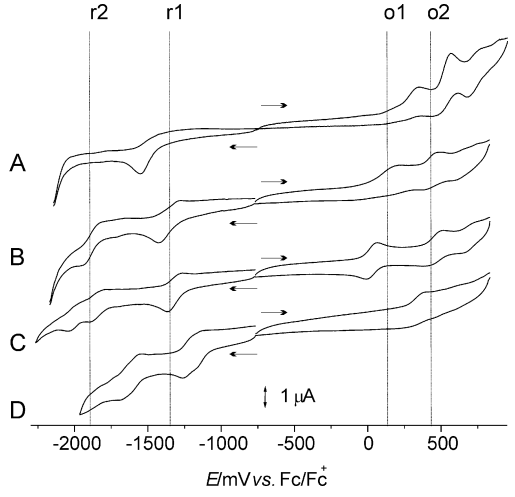

Figure 10. Cyclic voltammograms of **1**-[3′,5′-$(MeO)_2$] (A), **2** (B), **4** (C), and **5** (D). All experiments were performed in dichloromethane with tetrabutylammonium perchlorate as the supporting electrolyte, and glassy carbon, platinum wire, and Ag/AgCl as the working, auxiliary, and reference electrodes, respectively. The starting potentials and directions of the scans are marked with arrows. The vertical lines mark the wave potentials of the mactrocycle **2**.

the subunits of the dimeric complex **5** can be observed on the first and second reduction waves (Figure 10D). Both r1 and r2 are anodically shifted with respect to those of **2** due to the cationic character of the silver(I)-bridged system and split into two couples (–1172, –1303 and –1672, –1770 mV). The splitting of the waves reflects the effect of electron addition to one of the subunits of the dimeric molecule on the energy of the second subunit. Such an interaction may be either electronic (i.e., transferred by a conjugated bond system) or electrostatic (purely coulombic). In the case of no interaction between the subunits, no splitting is observed, and both subunits are reduced/oxidized at the same potential. Interactions of both types have been observed previously for covalently linked dimeric complexes of N-confused porphyrin derivatives.[12a,12b,21] Herein we have demonstrated for the first time an electrostatic interaction between organic subunits linked by coordination to the metal cation.

Conclusions

We have shown that acid-catalyzed ring fusion occurs chemo- and regiospecifically for *meso*-tetrakis(3′,5′-dimethoxyphenyl)NCP and involves the external carbon atom of the confused ring and the *ortho*-carbon atom of the adjacent aryl substituent. The resulting macrocycle remains aromatic and retains some of the coordination properties of N-confused porphyrin showing, however, some new features. The tendency towards a supramolecular assembly observed for protonated and metalated systems seems to be related to the presence of the exocyclic ring because no such association has been observed for analogous compounds without a fused ring. A stacking-type interaction between the extended π-electron systems of the subunits may be responsible for the stabilization of the oligomers.

Experimental Section

Instrumentation: Absorption spectra were recorded with a Varian Cary 50 Bio spectrophotometer. Mass spectra were recorded with a Bruker MicrOTOF-Q spectrometer by using the electrospray ionization technique. NMR spectra were recorded with Bruker Avance 500 and 600 spectrometers. 1D and 2D experiments (COSY, NOESY, ROESY, HMQC, and HMBC) were performed by standard experimental procedures of the Bruker library. Peaks were referenced to the residual $CHCl_3$ resonances in ^1H and ^{13}C NMR (δ =7.24 and 77.2 ppm, respectively). Diffusion experiments (DOSY) were performed with a Bruker Avance 600 NMR spectrometer with a 5 mm BBI probe head and equipped with a pulsed field gradient unit capable of producing magnetic field gradients in the *z* direction of about 5.35 G cm^{-1}. All experiments were carried out at 300 K in $CDCl_3$. The bipolar magnetic field pulse gradients (δ) were of 2.5–4.5 ms duration, and the diffusion time (Δ) was 50 ms. The pulse gradients were increased from 0.10 to 5.08 G cm^{-1} in 16 steps. Signals were averaged over 32 scans.

Preparation of the Precursors: The *meso*-tetraaryl-2-aza-21-carbaporphyrins **1** were synthesized according to a known procedure[5b] by using appropriate aromatic aldehydes.

5,10,15,20-Tetrakis(3,5-dimethoxyphenyl)-3,2′-cyclopenta-2-aza-21-carbaporphyrin (2): Trifluoroacetic acid was added in one portion (100 μL, 1.298 mmol) to a solution of **1**-[3′,5′-$(MeO)_2$] (80 mg, 0.0936 mmol) in toluene (30 mL). The solution was heated at reflux under dry aerobic conditions for 5 h. The color of the solution turned from brown-red to an intense red-purple after about 1 h. After the reaction was completed, the mixture was deacidified by vigorous stirring with wet potassium carbonate, filtered, and passed through a basic alumina column (activity III). The first red-brown band eluted with toluene contained a small amount of unreacted **1**-[3′,5′-$(MeO)_2$]. The fraction containing **2** was eluted with a toluene/dichloromethane mixture (1:3). The solid product was obtained from dichloromethane as a ruby powder by the addition of hexane and dried in vacuo. Yield: 55 mg (69%). Selected data: UV/Vis (CH_2Cl_2): λ_{max} (log ε) = 272 (4.35), 296 (sh), 401 (4.68), 466 (sh), 489 (4.81), 520 (4.56), 581 (sh), 643 (3.58), 699 (3.50), 788 (3.31 м$^{-1}$ cm^{-1}) nm. ^1H NMR (500 MHz, $CDCl_3$, 298 K, TMS): δ = 8.20 (d, ^3J = 5.2 Hz, 1 H, 7-H), 7.92 (d, ^3J = 4.6 Hz, 1 H, 18-H), 7.89 (d, ^3J = 5.2 Hz, 1 H, 8-H), 7.86 (d, ^3J = 4.6 Hz, 1 H, 13-H), 7.71 (d, ^3J = 4.9 Hz, 1 H, 12-H), 7.58 (d, ^3J = 4.3 Hz, 1 H, 17-H), 7.20 (d, ^4J = 2.1 Hz, 2 H, *o*-20), 7.02 (d, ^4J = 2.1 Hz, 2 H, *o*-15), 6.95 (d, ^4J = 2.4 Hz, 2 H, *o*-10), 6.75 (d, ^4J = 1.8 Hz, 1 H, *o*-5), 6.71 (t, ^4J = 2.1 Hz, 1 H, *p*-15), 6.69 (t, ^4J = 1.8 Hz, 1 H, *p*-10), 6.68 (t, ^4J = 1.9 Hz, 1 H, *p*-20), 5.83 (d, ^4J = 1.5 Hz, 1 H, *p*-5), 3.93 (s, 6 H, 2 × OMe), 3.92 (s, 3 H, OMe), 3.87 (s, 6 H, 2 × OMe), 3.86 (s, 6 H, 2 × OMe), 3.85 (s, 3 H, OMe), 2.27 (br. s, 1 H, 22-NH), 1.95 (br. s, 1 H, 24-NH), –0.63 (s, 1 H, 21-H) ppm. ^{13}C NMR (126 MHz, $CDCl_3$, 298 K): δ = 178.7, 165.4, 161.4, 159.5, 159.2, 158.5, 156.2, 154.6, 147.7, 143.1, 142.6, 141.1, 139.3, 139.2, 137.7, 135.7, 132.3, 129.9, 128.0, 125.9, 124.4, 123.8, 123.2, 120.0, 115.9, 115.2, 115.0, 112.6, 112.3, 112.2, 106.1, 104.5, 101.2, 100.3, 99.8, 97.9, 56.1, 55.6, 55.5, 55.5, 55.3 ppm. HRMS (ESI+; $CHCl_3$): calcd. for [$C_{52}H_{44}N_4O_8$ + H] 853.3237; found 853.3201. $C_{52}H_{44}N_4O_8 \cdot (CH_2Cl_2)_{0.25}$ (873): calcd. C 71.80, H 5.09, N 6.25; found C 71.79, H 5.13, N 6.41.

5,10,15,20-Tetrakis(3,5-dimethoxyphenyl)-3,2′-cyclopenta-2-aza-21-carbaporphyrinatonickel(II) (4): Nickel(II) acetate tetrahydrate (50 mg, 0.2 mmol) in ethanol solution (10 mL) was added to a solution of **2** (20 mg, 0.023 mmol) in toluene (30 mL), and the reaction mixture was heated at reflux under nitrogen for 12 h. The solvents were then removed, and the solid residue was extracted with dichloromethane and passed through a silica gel column. The first purple-red band was collected, and the product was precipitated from the solution by the addition of hexane and filtered. Yield: 15 mg (72%). Selected data for **4**: UV/Vis (CH_2Cl_2): λ_{max} (log ε) = 273 (sh), 391 (4.67), 452 (4.42), 494 (sh), 516 (4.65), 634 (3.80), 693 (4.17 м$^{-1}$ cm^{-1}) nm. ^1H NMR (600 MHz, $CDCl_3$, 298 K): δ = 7.60 (s, 1 H, 2-NH), 7.34 (d, ^3J = 5.2 Hz, 1 H, 7-H), 7.22 (d, ^3J = 5.2 Hz, 1 H, 8-H), 7.15 (d, ^3J = 5.0 Hz, 1 H, 18-H), 7.13 (d, ^3J = 4.7 Hz, 1 H, 13-H), 7.05 (d, ^3J = 5.0 Hz, 1 H, 12-H), 6.95 (d, ^3J = 4.7 Hz, 1 H, 17-H), 6.72 (d, ^4J = 2.3 Hz, 2 H, *o*-15), 6.71 (d, ^4J = 2.2 Hz, 2 H, *o*-20), 6.71 (d, ^4J = 2.3 Hz, 2 H, *o*-10), 6.58 (t, ^4J = 2.3 Hz, 1 H, *p*-20), 6.56 (t, ^4J = 2.2 Hz, 1 H, *p*-10), 6.55 (t, ^4J = 2.3 Hz, 1 H, *p*-15), 5.99 (d, ^4J = 1.7 Hz, 1 H, *o*-5), 5.28 (d, ^4J = 1.7 Hz, 1 H, *p*-5), 3.84 (s, 6 H, 20-OMe), 3.80 (s, 6 H, 10-OMe), 3.78 (s, 6 H, 15-OMe), 3.65 [s, 3 H, 5(5′)-OMe], 3.60 [s, 3 H, 5(3′)-OMe] ppm. ^{13}C NMR (151 MHz, $CDCl_3$, 298 K): δ = 167.5, 167.0, 159.9, 159.5, 159.5, 158.3, 157.8, 154.2, 153.3, 150.1, 147.2, 146.6, 144.3, 142.9, 142.8, 142.6, 141.0, 138.3, 133.5, 130.3, 128.3, 127.3, 125.9, 125.4, 123.6, 120.7, 120.5, 116.7, 116.7, 110.9, 110.4, 109.9, 108.3, 100.4,

99.8, 99.7, 96.5, 55.6, 55.5, 55.4, 55.2 ppm. HRMS (ESI): calcd. for $C_{52}H_{42}N_4NiO_8$ 908.2355; found 908.2333.

Bis[5,10,15,20-Tetrakis(3,5-dimethoxyphenyl)-3,2′-cyclopenta-2-aza-21-carbaporphyrin]silver(I) Tetrafluoroborate (5): A sample of **2** (15 mg, 0.017 mmol) was dissolved in chloroform (5 mL), and $AgBF_4$ (3.5 mg, 0.017 mmol) was add to the solution. The dark-purple solution formed was stirred at room temperature for 1 h. The reaction mixture was then washed with two portions of water (2 mL each), and the solvent was evaporated at room temperature. The solid residue was dissolved in chloroform and filtered. The orange-red product **5** was crystallized from chloroform/hexane. Yield: 13 mg (70%). Selected data for **5**: UV/Vis (CH_2Cl_2): λ_{max} ($\log\varepsilon$) = 275 (4.65), 321 (4.59), 402 (4.88), 480 (sh), 505 (5.02), 529 (sh), 591 (sh), 646 (3.86), 719 (3.65), 814 (3.60), 905 (3.47 $M^{-1}cm^{-1}$) nm. ^{1}H NMR (600 MHz, $CDCl_3$, 298 K): δ = 8.33 (d, ^3J = 5.1 Hz, 1 H, 7-H), 8.04 (d, ^3J = 5.1 Hz, 1 H, 8-H), 7.88 (d, ^3J = 4.7 Hz, 1 H, 13-H), 7.77 (d, ^3J = 4.7 Hz, 1 H, 12-H), 7.48 (d, ^3J = 4.5 Hz, 1 H, 17-H), 7.47 (d, ^3J = 4.5 Hz, 1 H, 18-H), 7.14 (dd, ^4J = 2.2, ^4J = 1.4 Hz, 1 H, *o*′-15), 6.98 (dd, ^4J = 2.1, ^4J = 1.4 Hz, 1 H, *o*-10), 6.96 (dd, ^4J = 2.2, ^4J = 1.5 Hz, 1 H, *o*′-10), 6.91 (dd, ^4J = 2.2, ^4J = 1.5 Hz, 1 H, *o*′-20), 6.80 (d, ^4J = 1.9 Hz, 1 H, *o*-5), 6.77 (dd, ^4J = 2.1, ^4J = 1.5 Hz, 1 H, *o*-15), 6.74 (t, ^4J = 2.2 Hz, 1 H, *p*-10), 6.69 (t, ^4J = 2.3 Hz, 1 H, *p*-15), 6.09 (dd, ^4J = 2.3, ^4J = 1.4 Hz, 1 H, *o*-20), 6.05 (d, ^4J = 1.4 Hz, 1 H, *p*-5), 5.76 (t, ^4J = 2.2 Hz, 1 H, *p*-20), 4.02 (s, 3 H, 5-OMe), 4.01 (s, 3 H, 5-OMe), 3.91 (s, 3 H, 10-OMe), 3.90 (s, 3 H, 10-OMe), 3.90 (s, 3 H, 15-OMe), 3.79 (s, 3 H, 15-OMe), 3.67 (s, 3 H, 20-OMe), 2.17 (br., 1 H, 22-NH), 2.10 (br., 1 H, 24-NH), 1.38 (s, 3 H, 20-OMe), –0.72 (s, 1 H, 21-H) ppm. ^{13}C NMR (126 MHz, $CDCl_3$, 298 K): δ = 176.2, 167.9, 162.5, 160.5, 159.9, 159.7, 159.3, 159.3, 156.0, 155.6, 154.4 (d, $J_{Ag,C}$ = 6.4 Hz), 146.2 (d, $J_{Ag,C}$ = 6.4 Hz), 142.4 (d, $J_{Ag,C}$ = 4.7 Hz, C-20), 141.9, 139.6, 138.4, 137.1, 136.6, 136.3, 133.3, 131.2, 127.3, 126.1, 125.2, 124.9, 124.0, 117.9, 117.5, 114.9, 114.0, 112.5, 112.4, 112.3, 109.5 (d, $^3J_{Ag,C}$ = 4.6 Hz, C-21), 108.2, 100.3, 100.0, 98.0, 97.2, 56.5, 55.8, 55.6, 55.5, 55.4, 53.6 ppm. HRMS (ESI): calcd. for $C_{104}H_{88}AgN_8O_{16}$ 1811.5369; found 1811.5349.

Calculations: DFT calculations were performed with the GAUSSIAN03 program.[14] Geometry optimizations were carried out within unconstrained C_1 symmetry with the starting coordinates derived from the MM+ model. Becke's three-parameter exchange functionals[22] with the gradient-corrected correlation formula of Lee–Yang–Parr [DFT(B3LYP)][23] were used with the 6-31G** basis set.[24] Harmonic vibrational frequencies were calculated for **2** by using analytical second derivatives. Structures were found to have converged to a minimum on the potential energy surface. ^{1}H and ^{13}C NMR chemical shifts and NICS (nuclear-independent chemical shift)[25] values were calculated by the GIAO (gauge-independent atomic orbitals) method[26] at the same level of theory. Natural population analysis (NPA) was performed by using the NBO program[27] at the same level of theory.

Supporting Information (see footnote on the first page of this article): 1D and 2D homo- and heteronuclear NMR spectra, UV/Vis and ^{1}H NMR titrations of **2** with TFA, calculation details, atomic Cartesian coordinates of the models, and correlation diagrams of calculated versus experimental chemical shifts.

Acknowledgments

Financial support from the Ministry of Science and Higher Education (Grant PBZ-KBN-118/T09/2004) is kindly acknowledged.

[1] S. Fox, R. W. Boyle, *Tetrahedron* **2006**, *62*, 10039.
[2] a) L. Barloy, D. Dolphin, D. Dupre, T. P. Wijesekera, *J. Org. Chem.* **1994**, *59*, 7976; b) S. Fox, R. W. Boyle, *Chem. Commun.* **2004**, 1322; c) C. Jeandon, R. Ruppert, S. Richeter, H. J. Callot, *Org. Lett.* **2003**, *5*, 1487; d) S. Richeter, C. Jeandon, R. Ruppert, H. J. Callot, *Tetrahedron Lett.* **2001**, *42*, 2103; e) J. Fouchet, C. Jeandon, R. Ruppert, H. J. Callot, *Org. Lett.* **2005**, *7*, 5257; f) S. Richeter, C. Jeandon, N. Kyritsakas, R. Ruppert, H. J. Callot, *J. Org. Chem.* **2003**, *68*, 9200; g) E. Hao, F. R. Fronczek, M. G. H. Vicente, *J. Org. Chem.* **2006**, *71*, 1233.
[3] a) A. Tsuda, Y. Nakamura, A. Osuka, *Chem. Commun.* **2003**, 1096; b) A. Tsuda, A. Nakano, H. Furuta, H. Yamochi, A. Osuka, *Angew. Chem. Int. Ed.* **2000**, *39*, 558; c) A. Tsuda, A. Osuka, *Adv. Mater.* **2002**, *14*, 75; d) M. G. H. Vicente, M. T. Cancilla, C. B. Lebrilla, K. M. Smith, *Chem. Commun.* **1998**, 2355; e) L. Jaquinod, O. Siri, R. G. Khoury, K. M. Smith, *Chem. Commun.* **1998**, 1261.
[4] P. J. Chmielewski, L. Latos-Grażyński, K. Rachlewicz, T. Głowiak, *Angew. Chem. Int. Ed. Engl.* **1994**, *33*, 779.
[5] a) H. Furuta, T. Asano, T. Ogawa, *J. Am. Chem. Soc.* **1994**, *116*, 767; b) G. R. Geier III, D. M. Haynes, J. S. Lindsey, *Org. Lett.* **1999**, *1*, 1455.
[6] a) H. Furuta, T. Ishizuka, A. Osuka, T. Ogawa, *J. Am. Chem. Soc.* **1999**, *121*, 2945; b) H. Furuta, T. Ishizuka, A. Osuka, T. Ogawa, *J. Am. Chem. Soc.* **2000**, *122*, 5748.
[7] Z. Xiao, B. O. Patrick, D. Dolphin, *Chem. Commun.* **2002**, 1816.
[8] P. J. Chmielewski, *Org. Lett.* **2005**, *7*, 1789.
[9] a) X. Li, P. J. Chmielewski, J. Xiang, J. Xu, Y. Li, H. Liu, D. Zhu, *Org. Lett.* **2006**, *8*, 1137; b) X. Li, P. J. Chmielewski, J. Xiang, J. Xu, L. Jiang, Y. Li, H. Liu, D. Zhu, *J. Org. Chem.* **2006**, *71*, 9739.
[10] a) T. Ishizuka, S. Ikeda, M. Toganoh, I. Yoshida, Y. Ishikawa, A. Osuka, H. Furuta, *Tetrahedron* **2008**, *64*, 4037; b) M. Toganoh, T. Kimura, H. Furuta, *Chem. Commun.* **2008**, 102.
[11] A. Młodzianowska, L. Latos-Grażyński, L. Szterenberg, *Inorg. Chem.* **2008**, *47*, 6364.
[12] a) P. J. Chmielewski, *Angew. Chem. Int. Ed.* **2004**, *43*, 5655; b) P. J. Chmielewski, *Angew. Chem. Int. Ed.* **2005**, *44*, 6417; c) M. Siczek, P. J. Chmielewski, *Angew. Chem. Int. Ed.* **2007**, *46*, 7432.
[13] I. Schmidt, P. J. Chmielewski, *Tetrahedron Lett.* **2001**, *42*, 1151.
[14] M. J. Frisch, G. W. Trucks, H. B. Schlegel, G. E. Scuseria, M. A. Robb, J. R. Cheeseman, V. G. Zakrzewski, J. A. Montgomery, R. E. Stratmann, J. C. Burant, S. Dapprich, J. M. Millam, A. D. Daniels, K. N. Kudin, M. C. Strain, O. Farkas, J. Tomasi, V. Barone, M. Cossi, R. Cammi, B. Mennucci, C. Pomelli, C. Adamo, S. Clifford, J. Ochterski, G. A. Petersson, P. Y. Ayala, Q. Cui, K. Morokuma, D. K. Malick, A. D. Rabuck, K. Raghavachari, J. B. Foresman, J. Cioslowski, J. V. Ortiz, B. B. Stefanov, G. Liu, A. Liashenko, P. Piskorz, I. Komaromi, R. Gomperts, R. L. Martin, D. J. Fox, T. Keith, M. A. Al-Laham, C. Y. Peng, A. Nanayakkara, C. Gonzales, M. Challacombe, P. M. W. Gill, B. G. Johnson, W. Chen, M. W. Wong, J. L. Andres, M. Head-Gordon, E. S. Replogle, J. A. Pople, *Gaussian03*, Revision C.01, Pittsburgh, PA, **2004**.
[15] P. J. Chmielewski, L. Latos-Grażyński, *J. Chem. Soc. Perkin Trans. 2* **1995**, 503.
[16] H. Furuta, T. Ishizuka, A. Osuka, H. Dejima, H. Nakagawa, Y. Ishikawa, *J. Am. Chem. Soc.* **2001**, *123*, 6207.
[17] G. Bringmann, S. Rüdenauer, D. G. C. Götz, T. A. M. Gulder, M. Reichert, *Org. Lett.* **2006**, *8*, 4743.
[18] P. J. Chmielewski, *Inorg. Chem.* **2009**, *48*, 432.
[19] H. Furuta, T. Ogawa, Y. Uwatoko, K. Araki, *Inorg. Chem.* **1999**, *38*, 2676.
[20] a) R. S. K. Kishore, T. Paululat, M. Schmittel, *Chem. Eur. J.* **2006**, *12*, 8136; b) L. Allouche, A. Marquis, J.-M. Lehn, *Chem. Eur. J.* **2006**, *12*, 7520.
[21] a) I. Schmidt, P. J. Chmielewski, *Inorg. Chem.* **2003**, *42*, 5579; b) P. J. Chmielewski, *Inorg. Chem.* **2007**, *46*, 1617.
[22] A. D. Becke, *Phys. Rev. A* **1988**, *38*, 3098.

[23] C. Lee, W. Yang, R. G. Parr, *Phys. Rev. B* **1988**, *37*, 785.
[24] P. J. Hay, W. R. Wadt, *J. Chem. Phys.* **1985**, *82*, 270; P. J. Hay, W. R. Wadt, *J. Chem. Phys.* **1985**, *82*, 284; P. J. Hay, W. R. Wadt, *J. Chem. Phys.* **1985**, *82*, 270; P. J. Hay, W. R. Wadt, *J. Chem. Phys.* **1985**, *82*, 299.
[25] P. v. R. Schleyer, C. Meaerker, A. Dransfeld, H. Jiao, N. J. R. v. E. Hommes, *J. Am. Chem. Soc.* **1996**, *118*, 6317.
[26] K. Wolinski, J. F. Hinton, P. Pulay, *J. Am. Chem. Soc.* **1990**, *112*, 8251.
[27] E. D. Glendening, A. E. Reed, J. E. Carpenter, F. Weinhold, Theoretical Chemistry Institute, University of Wisconsin, Madison, *NBO, Version 3.1* (included in the Gaussian 03 package of programs), Gaussian, Inc., Wallingford, CT, **2004**.

Received: March 28, 2009
Published Online: July 6, 2009

